RSC Advances

PAPER

View Article Online
View Journal | View Issue

Cite this: *RSC Adv.*, 2024, **14**, 25120

Bent naphthodithiophenes: synthesis and characterization of isomeric fluorophores†

Emmanuel B. A. Adusei, [a] Vincent T. Casetti,[a] Calvin D. Goldsmith, [a] Madison Caswell,[a] Drecila Alinj, [a] Jimin Park, [a] Matthias Zeller, [b] Alexander A. Rusakov [a] and Zacharias J. Kinney *[a]

Thiophene-containing heteroarenes are one of the most well-known classes of π-conjugated building blocks for photoactive molecules. Isomeric naphthodithiophenes (NDTs) are at the forefront of this research area due to their straightforward synthesis and derivatization. Notably, NDT geometries that are bent – such as naphtho[2,1-*b*:3,4-*b*′]dithiophene (α-NDT) and naphtho[1,2-*b*:4,3-*b*′]dithiophene (β-NDT) – are seldom employed as photoactive small molecules. This report investigates how remote substituents impact the photophysical properties of isomeric α- and β-NDTs. The orientation of the thiophene units plays a critical role in the emission: in the **α(OHex)R$_2$** series conjugation from the end-caps to the NDT core is apparent, while in the **β(O*i*-Pent)R$_2$** series minimal change is observed unless strong electron acceptors, such as **β(O*i*-Pent)(PhCF$_3$)$_2$**, are employed. This push–pull acceptor–donor–acceptor (A–D–A) fluorophore exhibits positive fluorosolvatochromism that correlates with increasing solvent polarity parameter, $E_T(30)$. In total, these results highlight how remote substituents are able to modulate the emission of isomeric bent NDTs.

Received 4th July 2024
Accepted 26th July 2024

DOI: 10.1039/d4ra04850d

rsc.li/rsc-advances

1 Introduction

Heteroarenes, polyaromatic hydrocarbons (PAHs) bearing main group elements, are well established as building blocks for π-conjugated functional materials.[1–4] Thiophene-containing heteroarenes with benzene, naphthalene, or anthracene cores have been thoroughly investigated as electron rich moieties within both small molecule and polymer systems with applications in organic electronics.[1,5,6] Of the thiophene-based heteroarenes, naphthodithiophenes (NDTs) are of particular interest due to the plethora of isomers available and their straightforward derivatization.[7,8] Linear and angular NDTs shown in Fig. 1a represent two classes of isomeric NDTs that have found applications throughout organic electronics, most notably as organic field-effect transistors (OFETs),[9–11] organic light-emitting diodes (OLEDs),[12] organic[13,14] and dye-sensitized[15] solar cells, and more recently as hole-transporting materials (HTMs).[12,16,17] Due to the orientation of the residual α-positions (2- and 7-positions, labelled in Fig. 1a), NDT-1 and NDT-2 are considered to be linear rods, while NDT-3 and NDT-4 are described as angular.[7]

Alternatively bent NDTs – such as naphtho[2,1-*b*:3,4-*b*′]dithiophene (α-NDT) and naphtho[1,2-*b*:4,3-*b*′]dithiophene (β-NDT) shown in Fig. 1b – are known building blocks in polymeric materials,[18,19] but are underrepresented as luminescent small molecules.[16,20] At their core, unfunctionalized α- and β-NDTs are isoelectronic to triphenylene, but can be easily fused to other motifs to yield electron deficient cores (*e.g.* phenazines[21] or imides[19,22]). The α-positions of α- and β-NDTs, labelled in Fig. 1b, offer a facile means to modulate the emissive properties of the core *via* peripheral derivatization (*i.e.* V-shaped[23] acceptor–donor–acceptor systems). These bent push–pull fluorophores[24] are reminiscent of Höger and co-workers isomeric dithienylphenazines (termed α- and β-DTPs), whose systems

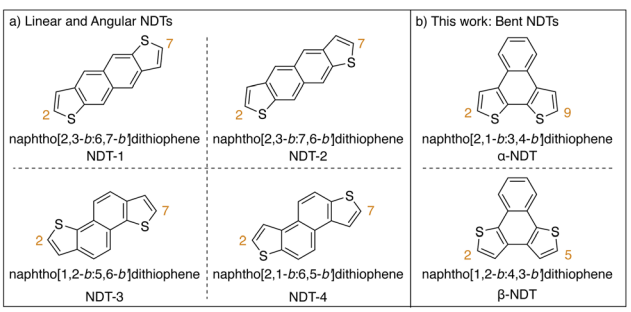

Fig. 1 Classes of naphthodithiophenes. (a) Isomeric linear and angular naphthodithiophenes. (b) This work: isomeric bent naphthodithiophenes.

[a]*Department of Chemistry, Oakland University, Rochester, Michigan, USA. E-mail: kinney@oakland.edu; Tel: +1-248-370-2347*

[b]*Department of Chemistry, Purdue University, West Lafayette, Indiana, USA*

† Electronic supplementary information (ESI) available: Experimental procedures, NMR and photophysical spectra, supplemental figures and analysis referred to in the text, computational data, and crystallographic results. CCDC 2361476–2361480. For ESI and crystallographic data in CIF or other electronic format see DOI: **https://doi.org/10.1039/d4ra04850d**

have inverted electronics (*i.e.* the electronics are aligned to be donor–acceptor–donor systems). Their series of α- and β-DTPs were shown to have variable conjugation paths based on the isomer employed, ultimately yielding photoactive molecules that are fluorescent (α-DTP) or dual emitters (β-DTP).[25,26] With this in mind, probing how the peripheral functionalization of α- and β-NDTs impacts the photoactive cores – and ultimately their application as push–pull fluorophores – is of interest.

Herein we investigate the structure–property relationships in a series of isomeric bent NDTs – naphtho[2,1-*b*:3,4-*b*′]dithiophene (α-NDT) and naphtho[1,2-*b*:4,3-*b*′]dithiophene (β-NDT) – with variable end-caps. The initial premise of this research effort was to establish if the peripheral **R**-groups are (1) in communication with the NDT core and (2) if there are distinct differences between the isomers. NMR spectroscopy can afford preliminary evidence of communication to the core in the ground state *via* modulation of interior resonances far removed from the **R**-groups; while emission spectra are informative of excited state communication. Ultimately, there are clear differences in the photophysical properties between the isomers, with α-NDT being more receptive to all types of peripheral substituents and β-NDT only being responsive to electron-deficient end-caps.

2 Results and discussion

2.1 α(OR′)R_2 series: synthesis and structural analysis

With the goal of having both solution- and solid-state metrics for the **α(OR′)R_2** series two monomers with differing solubility are needed. For the solution-state analysis, hexyloxy groups were used to ensure that all α-NDT derivatives are soluble across a range of concentrations, particularly with aggregation being a concern for similar PAH systems.[27] To investigate solid-state metrics methoxy groups were used to maximize the chance of growing single crystals for X-ray diffraction. Both **α(OHex)R_2** and **α(OMe)R_2** can be synthesized *via* a streamlined bottom-up approach. Scheme 1 details the synthetic path to the **α(OHex)R_2** series beginning with the alkylation of 4,5-dibromocatechol[28] with iodohexane to yield solubilized building block **1(OHex)**. Installation of the thiophene units is accomplished *via* palladium-mediated cross-coupling to afford **2(OHex)** in modest yield. Planarization of **2(OHex)** under typical Scholl oxidation conditions[29] affords **α(OHex)** as an off-white crystalline solid after column purification. Bromination of the open α-positions with NBS yields **α(OHex)Br_2**, a versatile core molecule for attaching end-caps with variable electronic properties. Commercially available phenyl boronic acid (**R = Ph**, H σ_p = 0.00) and *para*-functionalized phenyl boronic acid derivatives *p*-tolyl boronic acid (**R = Tol**, Me $\sigma_p = -0.17$), *p*-methoxyphenyl boronic acid (**R = PhOMe**, OMe $\sigma_p = -0.27$), and *p*-(trifluoromethyl)phenyl boronic acid (**R = PhCF$_3$**, CF_3 $\sigma_p = +0.54$) were chosen as end-caps due to their variable electronic properties that are poised to be in resonance with the NDT cores. Due to this arrangement for the **R**-groups Hammett parameters[30] for σ_p, which include resonance effects, are more informative than electronically isolated σ_m. Suzuki cross-coupling of the boronic acids proved to be efficient across all derivatives, with modest isolated yields for the **α(OHex)R_2** series (Scheme 1, inset).

The **α(OMe)R_2** series follows an identical synthetic path as **α(OHex)R_2** (shown in Scheme 1), with the exception of starting from 4,5-dibromoveratrole.[31] The solubility of the **α(OMe)R_2** series is demonstrably worse than the hexyloxy series, which proved challenging for purification and analysis (see ESI†). Due to this poor solubility the **α(OMe)R_2** series was used almost explicitly for crystallography. Single crystals of sufficient quality for X-ray diffraction were grown for each derivative *via* vapor diffusion of hexanes into saturated solutions of **α(OMe)R_2** in THF (see ESI†). Of particular interest are the inter-ring bond lengths, which can detail the level of communication the remote substituents have with the α-NDT core, and the supramolecular organization of the **α(OMe)R_2** series. The C–C linkage between the α-NDT core and the appended **R**-groups are expected to display minor elongation due to torsional strain between the ring systems (C–C ≈ 1.45 Å),[32] with measurements under this value being indicative of increased conjugation with the α-NDT core. Each **α(OMe)R_2** derivative has an inter-ring bond length of ≈1.46 Å, revealing negligible bond elongation with no dependence on the **R**-group. The herringbone arrays formed in the crystallographic packing of the **α(OMe)R_2** series reveal that the planar cores of the α-NDTs are arranged into slipped-stacks with arene–arene distances of ≈3.5 Å (see ESI† for full details).

With these solid-state metrics established, we turned our attention to the solubilized **α(OHex)R_2** derivatives for solution-state structural analysis. Specifically of interest are resonances far removed from the **R**-groups that are part of the NDT core, as these signals are expected to shift if there is communication from the end-caps to the core. The NDT cores themselves are electron-rich, therefore **R**-groups that are electron withdrawing are expected to function as intramolecular acceptor–donor–acceptor (A–D–A) systems, while electron-rich groups are expected to yield highly polarized all donor systems. Intramolecular A–D–A species are posited to increase the contribution of the quinoidal resonance, a highly desirable characteristic in photoactive molecules.[23] Key proton resonances 2b and 3b are highlighted in Fig. 2 and are matched between each derivative of the **α(OHex)R_2** series to ease comparison.

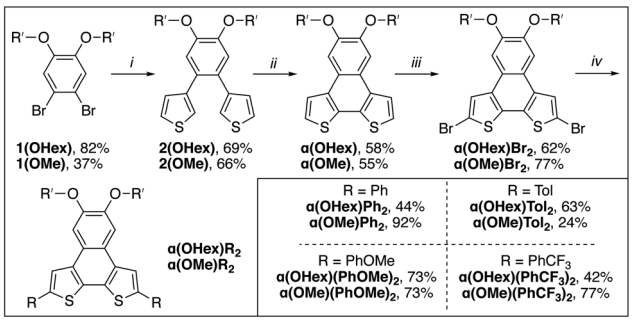

Scheme 1 Synthesis of α(OR′)R_2 series. (i) 3-thiophene boronic acid, $Pd(PPh_3)_2Cl_2$, 2 M K_2CO_3, THF, 80 °C, overnight; (ii) $FeCl_3$, $MeNO_2$, DCM, 0 °C to RT, 1 h; (iii) NBS, $CHCl_3$, RT, 2 d; (iv) **R** boronic acid, $Pd(PPh_3)_2Cl_2$, 2 M K_2CO_3, THF, 80 °C, overnight. (Inset): Isolated yields for **α(OHex)R_2** and **α(OMe)R_2** series.

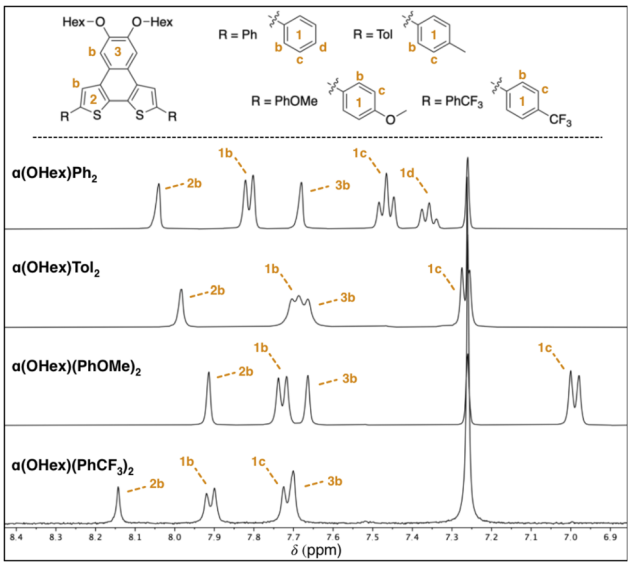

Fig. 2 Partial ^{1}H NMR spectra for the **α(OHex)R$_2$** series with assignment of aromatic resonances (400 MHz, $CDCl_3$). See ESI† for full spectra and assignments.

Due to the planar nature of the NDT cores aggregation is likely, thus comparison of NMR spectra at similar dilute concentrations is required. Inspection of the aromatic region of dilute (≤10 mM) solutions of each **α(OHex)R$_2$** species reveals slight perturbations of the interior 2b proton ($\Delta\delta \approx 0.20$ ppm, Fig. 2) and carbon ($\Delta\delta \approx 3$ ppm, see ESI†) resonances. Modulation of the 2b resonances is quite unique: these signals are far removed from the functional group and indicate that there is remote communication to the NDT core upon end-capping. Relative to parent **α(OHex)Ph$_2$** the electron donating groups shift the 2b resonance upfield with **α(OHex)Tol$_2$** ($\Delta\delta$ −0.06 ppm) and **α(OHex)(PhOMe)$_2$** ($\Delta\delta$ −0.13 ppm) both being above the threshold of significance ($\Delta\delta \geq 0.05$ ppm). **α(OHex)(PhCF$_3$)$_2$** is shifted downfield in comparison ($\Delta\delta$ +0.10 ppm), indicative of a shift towards a higher energy state (with respect to parent **α(OHex)Ph$_2$**). Overall, the shift differences observed for the 2b proton resonances are quite small ($\Delta\delta < 0.25$ ppm); thus, inspection of the ^{13}C signals for the 2b resonances could be informative. Indeed, the ^{13}C resonances follow the same trend, wherein **α(OHex)Tol$_2$** ($\Delta\delta$ −0.6 ppm) and **α(OHex)(PhOMe)$_2$** ($\Delta\delta$ −1.1 ppm) are shifted upfield relative to **α(OHex)Ph$_2$** and **α(OHex)(PhCF$_3$)$_2$** is shifted downfield ($\Delta\delta$ +1.6 ppm). This trend fits well with σ_p for the **R**-groups for both the observed ^{1}H and ^{13}C resonances of 2b, while σ_m yields poor fits (see ESI†). To ensure these observations are not artefacts of aggregation, a series of variable concentration solutions were probed for the **α(OHex)R$_2$** series (see ESI,† 50–1 mM in $CDCl_3$). These data for **α(OHex)Tol$_2$** and **α(OHex)(PhOMe)$_2$** suggest that there is minimal propensity for aggregation in $CDCl_3$ ($\Delta\delta \leq 0.12$ ppm for all resonances), with measured K_d of $\approx 3.2 \times 10^{-4}$ M and ≈ 1.2 M for these two derivatives respectively.[33,34]

To verify the attribution of the small perturbations observed *via* NMR to the remote **R**-groups, we modelled the NMR spectra of the **α(OHex)R$_2$** series computationally. To simplify simulations and clarify the assignment of NMR features, we replaced the hexyloxy groups with methoxy. To differentiate from the synthesized **α(OMe)R$_2$** series the model series is represented as α(OMe)R$_2$′. In our ^{1}H and ^{13}C calculated NMR spectra, we rely on the widely adopted non-relativistic density functional theory (DFT) protocol with gauge including atomic orbitals (GIAO)[35,36] as implemented in the Gaussian 16 (ref. 37) programme suite. The justification of the non-relativistic approach comes from the smallness of the heavy atom effect in compounds containing sulfur and lighter elements only.[38–42] In all DFT calculations, we use a popular global hybrid exchange–correlation functional (XCF) approximation B3LYP[43,44] widely regarded in the literature as a reliable choice[45–60] even in light of recent advances.[47,51,53,61–64] Finally, we choose to work with polarization-consistent basis sets developed by Jensen for rational and systematic reduction of basis-set error specifically in DFT methods.[65–67] In particular, we use pc-2 (ref. 68) for geometry optimizations and vibrational frequency calculations, and aug-pc-Sseg-2 (ref. 69) for modelling NMR spectra. The latter set belongs to the pc-Sseg-*n* family of basis sets augmented with additional tight exponents for the description of the electronic density near atomic nuclei and optimised for nuclear magnetic shielding. These sets have been known to markedly outperform other available choices for core-related properties.[70,71] Due to the poor solubility of **α(OHex)(PhCF$_3$)$_2$** – and the entire **α(OMe)R$_2$** series – only experimental resonances extracted from the ^{1}H–^{13}C HSQC

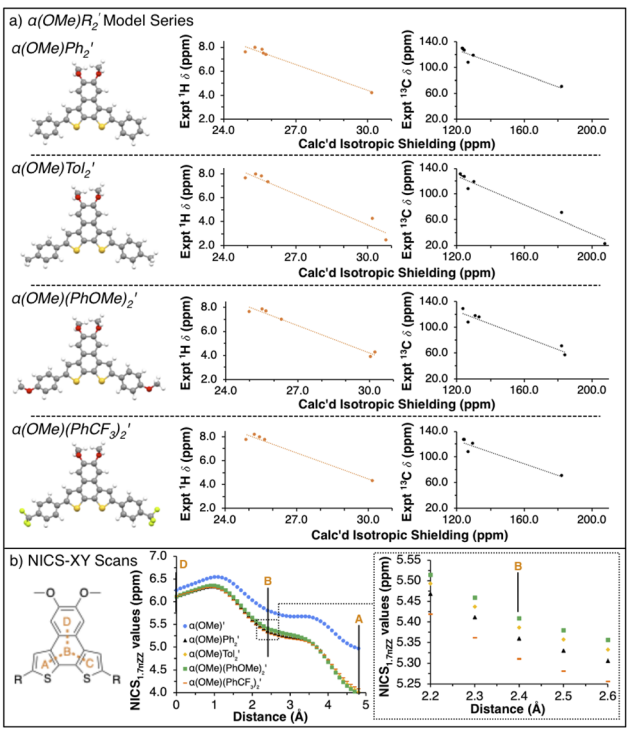

Fig. 3 Computational analysis of α(Me)R$_2$′ series. (a) Ball-and-stick representations of model compounds α(OMe)R$_2$′ and their respective experimental *vs.* calculated NMR plots (^{1}H is shown in orange, ^{13}C is given in black). (b) Partial $NICS_{1.7\pi ZZ}$ scans for α(OMe)R$_2$′ with D–B–A path highlighted in orange. (Inset): Enhanced view of the central B ring.

spectra were used for comparison to calculated parameters. Comparison of the ^{1}H and ^{13}C isotropic shieldings for the model α(OMe)R_2' series to the synthesized **α(OHex)R_2** (shown in Fig. 3) and **α(OMe)R_2** (see ESI†) series yield quality fits ($r^2 > 0.9$), further indicating that the modulation of the interior chemical shifts is directly related to the remote **R**-groups.

With the model α(OMe)R_2' series validated, we sought to probe how the **R**-groups impact the aromaticity of the α-NDT core. Nucleus independent chemical shift (NICS)[72] calculations are a well-known computational means to assess the aromatic (or antiaromatic) character of heteroarene systems.[73–75] Specifically, NICS-XY scans[76,77] wherein the ghost atom is set to 1.7 Å above the planar α-NDT core were performed to ascertain if there are electronic effects in the core that were not apparent *via* traditional spectroscopic means. In Fig. 3b, we detail the results of the NICS-XY scans for the α(OMe)R_2' series referenced against a model compounds without **R**-groups, α(OMe)′. The α(OMe)R_2' cores are weakly paratropic no matter the **R**-group ($NICS_{1.7\pi ZZ}$ values ≈4–6.5 ppm over the path of the probe); there are minor deviations in the 'B' ring that follow the Hammett parameter (σ_p specifically) of the **R**-group (*i.e.* there is an increase in aromatic character as the **R**-group becomes more electron deficient).

2.2 α(OHex)R_2 series: photophysical properties

Our focus shifted to elucidating the photophysical properties of the **α(OHex)R_2** series upon completion of their structural authentication. UV-visible absorption spectra for the **α(OHex)R_2** series, shown in Fig. 4a, display defined (despite being broadened) vibronic structure in-line with known α-NDT containing materials.[78] Table 1 highlights several key metrics of these data, where there is a slight bathochromic shift when progressing from **α(OHex)Ph$_2$** to stronger electron donating groups in **α(OHex)Tol$_2$** and **α(OHex)(PhOMe)$_2$** ($\Delta\lambda_{abs,max} \leq 5$ nm). The lone A–D–A system, **α(OHex)(PhCF$_3$)$_2$**, is quite distinct with a 12 nm bathochromic shift relative to parent **α(OHex)Ph$_2$**. The optical band gap ($E_{g,opt}$) was estimated from the tangent of the absorption onset, with **α(OHex)(PhCF$_3$)$_2$** having the smallest gap ($E_{g,opt}$ 2.89 eV). The emission spectra (Fig. 4b) have strong, detailed, vibronic structure.

The fine vibronic structure observed in the emission spectra are indicative of enhanced conjugation in the excited state through rigidification of the molecules (as compared to the relatively structure-less absorption spectra). For α-NDT containing molecules this implies stabilization (and an increase in) the quinoidal resonance contribution.[79] Photoluminescence quantum yield (Φ_{PL}) measurements were undertaken for each derivative under inert atmosphere in dry THF. **α(OHex)(PhOMe)$_2$** provided the highest quantum yield (Φ_{PL} ≈ 0.40) in THF, while **α(OHex)Ph$_2$** (Φ_{PL} ≈ 0.25), **α(OHex)Tol$_2$** (Φ_{PL} ≈ 0.25), and **α(OHex)(PhCF$_3$)$_2$** (Φ_{PL} ≈ 0.24) are within the error of the technique (±10%). These results are in agreement with known phenylene end-capped α-NDTs α(PhBu)$_2$ (Φ_{PL} ≈ 0.28)[20] and α(PhN(PhOMe)$_2$)$_2$ (Φ_{PL} ≈ 0.55).[16] Itami and co-workers posited that these photoactive molecules are suitable hole-transporting materials, which is an application we plan on pursuing in the future with solubilized α-NDTs. It is worth noting that the highly polarized all-donor systems containing anisole-based end-caps provided the highest quantum yields whether directly attached (**α(OHex)(PhOMe)$_2$**) or connected *via* an amine linkage (α(PhN(PhOMe)$_2$)$_2$).

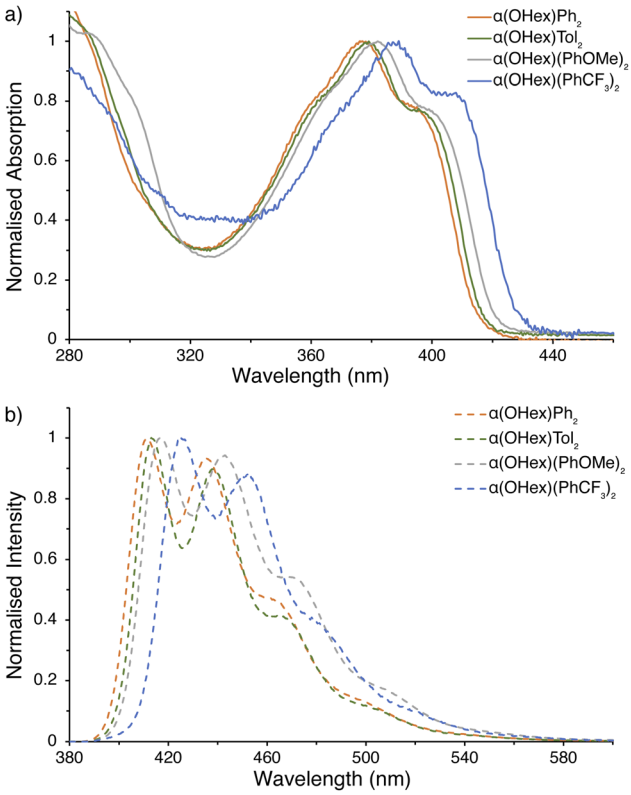

Fig. 4 Photophysical measurements for **α(OHex)R_2** series. (a) UV-visible spectra; (b) emission spectra (λ_{ex} = 365 nm). All samples were prepared under an inert atmosphere with degassed dry THF.

Table 1 **α(OHex)R_2** Series spectral data[a]

α(OR′)R_2	ε (M^{-1} cm^{-1})	$\lambda_{abs,max}$ (nm)	$E_{g,opt}$[b] (eV)	λ_{em}[c] (nm)	Φ_{PL}[c]
α(OHex)Ph$_2$	3.78×10^4	377	2.99	412	0.25
α(OHex)Tol$_2$	3.67×10^4	379	2.97	416	0.25
α(OHex)(PhOMe)$_2$	3.40×10^4	382	2.94	419	0.40
α(OHex)(PhCF$_3$)$_2$	1.18×10^4	389	2.89	427	0.24

[a] UV-visible and emission spectra were measured as solutions in dry, degassed THF under inert atmosphere. [b] $E_{g,opt}$ estimated from the tangent of the absorption onset, $\lambda_{abs,onset}$. [c] λ_{ex} = 365 nm.

2.3 β(O*i*-Pent)R_2 series: synthesis and structural analysis

The poor solubility of the **α(OHex)R_2** series led us to reconfigure the solubilizing groups for the β-NDT series to a short, branched alkoxy group that promotes solubility but still allows for crystallization. Alkylation of 4,5-dibromocatechol with *iso*-pentyl bromide efficiently affords **1(O*i*-Pent)** as a colorless oil that is converted to **3(O*i*-Pent)** *via* Suzuki cross-coupling with 2-thiophene boronic acid in modest yield on the gram scale

(Scheme 2). This is quite astonishing considering this boronic acid coupling partner is known to undergo moderate protodeborylation under traditional cross-coupling conditions.[80] Blocking of the unfunctionalized α-positions of the thienyl groups is required prior to planarization to mitigate polymerization (or rearrangement).[78,81] With this in mind, bromination[82] of the residual α-positions of **3(O*i*-Pent)** affords **4(O*i*-Pent)** in modest yield. In our hands traditional Scholl oxidation conditions were inefficient (yields < 10%) to planarize the brominated species, but organic oxidant and acidic conditions (DDQ, methanesulfonic acid, DCM)[82,83] proved to be far superior in accessing **β(O*i*-Pent)Br$_2$** in modest yield (>40% isolated yields on 500 mg scale).

End-capping of **β(O*i*-Pent)Br$_2$** with the aryl boronic acid derivatives yields the **β(O*i*-Pent)R$_2$** series as off-white to pale yellow solids. Exchanging the solubilizing groups for *iso*-pentyloxy resulted in an appreciable improvement in solubility, with all **β(O*i*-Pent)R$_2$** being soluble in common organic solvents (*e.g.* 50 mM in $CDCl_3$). The central goal of using the *iso*-pentyloxy groups is to thread the needle between solubility and the ability to grow single crystals for analysis. After several attempts with all derivatives, single crystals suitable for X-ray diffraction were grown *via* vapor diffusion of hexanes into a saturated solution of **β(O*i*-Pent)Tol$_2$** in THF. The crystal obtained for **β(O*i*-Pent)Tol$_2$** is dimeric, wherein the two units are aligned in the same direction with the β-NDT cores offset (*i.e.* a slip-stacked arene–arene stacking arrangement) with a distance between the dimers of ≈ 3.6 Å (see ESI†). The interring C–C bond length for **β(O*i*-Pent)Tol$_2$** is 1.46 Å, nearly identical to the same metrics obtained in the **α(OMe)R$_2$** series. However the crystallograhic packing of **β(O*i*-Pent)Tol$_2$** dimers into columnar stacks is distinct in comparison to the **α(OMe)R$_2$** series. This difference in crystallographic packing can brought back to the branch alkoxy solubilizing group of **β(O*i*-Pent)Tol$_2$**, which upon crystallization intercalate with adjacent stacks, thus allowing for columnar stacks of the dimers to form.

The partial aromatic region shown in Fig. 5 reveals the interior 2b proton resonance (as well as the ^{13}C resonance) is responsive to remote functionalization. These perturbations of

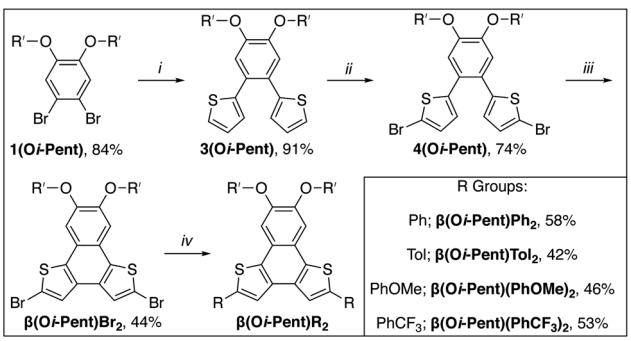

Scheme 2 Synthesis of **β(O*i*-Pent)R$_2$** series. (i) 2-Thiophene boronic acid, $Pd(PPh_3)_2Cl_2$, 2 M K_2CO_3, THF, 80 °C, overnight; (ii) NBS, $CHCl_3$, RT, 2 d; (iii) DDQ, $MeSO_3H$, DCM, 0 °C to RT, 1 h; (iv) **R** boronic acid, $Pd(PPh_3)_2Cl_2$, 2 M K_2CO_3, THF, 80 °C, overnight. Inset: isolated yields for **β(O*i*-Pent)R$_2$** series.

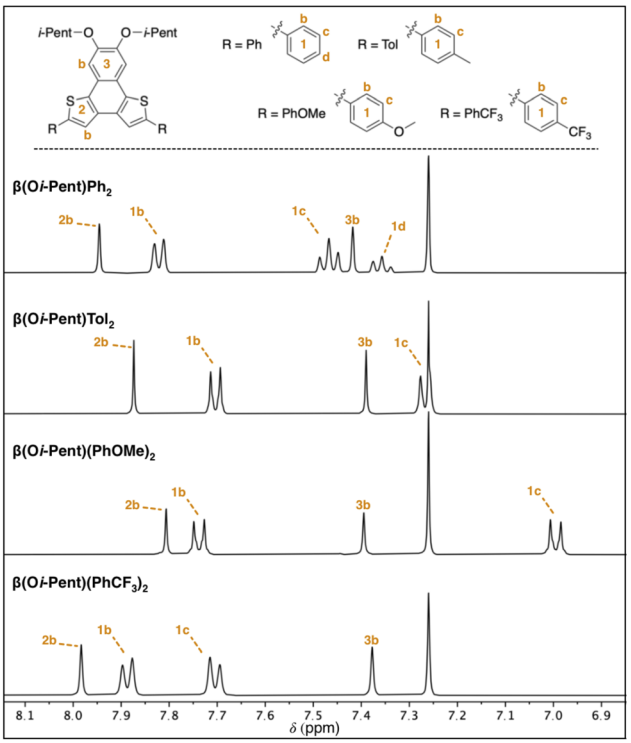

Fig. 5 Partial ^{1}H NMR spectra for the **β(O*i*-Pent)R$_2$** series with assignment of aromatic resonances (400 MHz, $CDCl_3$). See ESI† for full spectra and complete chemical shift assignments.

the 2b proton and carbon resonances are quite similar to those observed in the **α(OHex)R$_2$** series, with the **β(O*i*-Pent)R$_2$** series having $\Delta\delta \approx 0.2$ ppm for ^{1}H and $\Delta\delta \approx 2$ ppm for ^{13}C. Fitting these chemical shifts to both σ_p and σ_m Hammett parameters reveals a quality correlation to σ_p, albeit not as pure of a fit as with the **α(OHex)R$_2$** series. Although the **β(O*i*-Pent)R$_2$** derivates are quite soluble, one concern for the poor fit (r^2 0.7) for the ^{1}H spectra is aggregation. The orientation of the thiophene rings in the β-NDT isomer give the molecules a pronounced bent shape (the approximate bite angle of the terminal substituents is 110°) in comparison to the α series (bite angle ≈ 125°), which may impact their propensity for aggregation. Solutions of **β(O*i*-Pent)Tol$_2$** and **β(O*i*-Pent)(PhOMe)$_2$** in $CDCl_3$ were prepared and analyzed across a range of concentrations (50–1 mM, see ESI†) to probe this concern. Only chemical shifts in which $\Delta\delta \geq 0.05$ ppm were included in the fitting analysis,[33,34] revealing K_d values of 1.1 M and 1.5 M for **β(O*i*-Pent)Tol$_2$** and **β(O*i*-Pent)(PhOMe)$_2$**, respectively. These values are in-line with the **α(OHex)R$_2$** series, highlighting that the minor geometric differences in the bent NDTs do not impart vastly different aggregation potential.

Following the same computational methodology as the α-NDT series, model compounds bearing methoxy groups were used to calculate both the NMR spectra and perform NICS-XY scans. The model β-NDT series, β(OMe)R$_2'$, reveals that the experimental ^{1}H and ^{13}C resonances obtained from the ^{1}H–^{13}C HSQC spectra for each derivative yield quality fits ($r^2 > 0.9$) with the calculated isotropic shielding values (see ESI†). NICS-XY

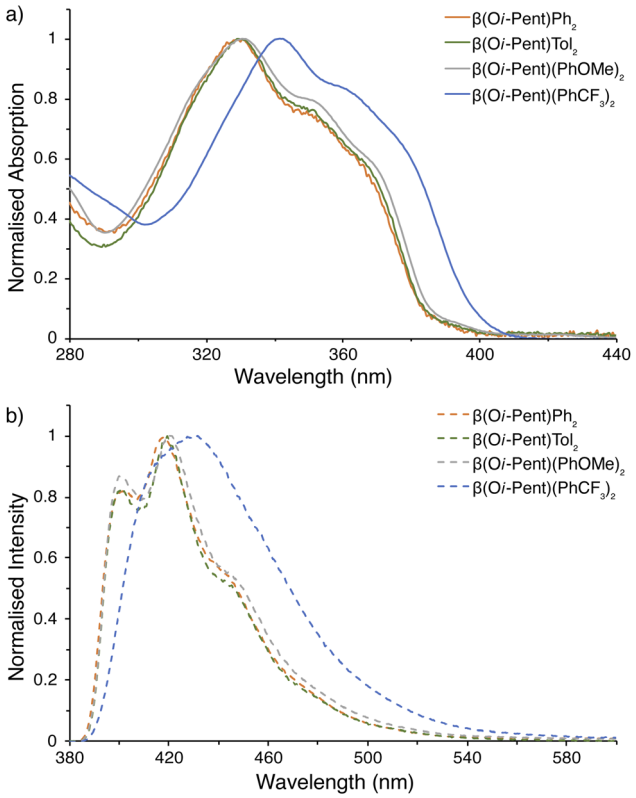

Fig. 6 Photophysical measurements for **β(O*i*-Pent)R_2** series. (a) UV-visible spectra; (b) emission spectra (λ_{ex} = 365 nm). All samples were prepared under inert atmosphere with degassed dry THF.

scans across the β-NDT core yields a similiar pattern to the α(OMe)R_2' series, with the central differences being the $NICS_{1.7\pi ZZ}$ values of the 'A' ring β(OMe)R_2' are ≈0.4 ppm lower than α(OMe)R_2'). The 'B' ring follows the same trend with σ_p, although the differences between each derivative are minute ($\Delta NICS_{1.7\pi ZZ}$ values ≈0.10 ppm, see ESI†).

2.3.1 β(O*i*-Pent)R_2 series: photophysical properties. The change in potential conjugation path between the α- and β-isomers opens the possibility of the β-NDT isomer to break the aromaticity of the upper aromatic ring (labelled as ring 3 in Fig. 5), as is observed in Höger and co-workers β-DTP system.[25,26] Disrupting this Clar sextet[84,85] is unlikely, thus conjugation from the **R**-groups to solely the thiophene units is expected. Fig. 6a details the UV-visible and emission spectra of the **β(O*i*-Pent)R_2** series, revealing the β-isomer to be quite different than the **α(OHex)R_2** series.

Critically, there are no discernible differences in the photophysical properties between the **β(O*i*-Pent)Ph_2**, **β(O*i*-Pent)Tol_2** and **β(O*i*-Pent)(PhOMe)$_2$** derivatives (Table 2). These derivatives have broadened vibronic structure in both the emission and excitation spectra. In contrast to their α-NDT series counterparts the **β(O*i*-Pent)Ph_2**, **β(O*i*-Pent)Tol_2** and **β(O*i*-Pent)(PhOMe)$_2$** derivatives have larger band gaps ($E_{g,opt}$ > 3.10 eV) and decreased Φ_{PL}, with **β(O*i*-Pent)(PhOMe)$_2$** having the largest difference between isomers at 20% below **α(OHex)(PhOMe)$_2$**. While there are, to the best of our knowledge, no directly comparable quantum yields in the literature for β-NDTs, this drop in quantum yield has been observed in scrambled bent NDTs (compound 2l Φ_{PL} = 0.03)[20] and with Miyazaki and co-workers 2,3-naphthalimide-fused benzodithiophenes (Φ_{PL} ≈ 0.03–0.09).[22] However, **β(O*i*-Pent)$(PhCF_3)_2$** is distinct in this analysis. The UV-visible spectrum is bathochromically shifted ($\lambda_{abs,max}$ = 11 nm) in comparison to the rest of the **β(O*i*-Pent)R_2** series with similar vibronic structure, but the emission spectrum is broadened and ill-defined (Fig. 6b).

This is in stark contrast to the rest of the **β(O*i*-Pent)R_2** series (and the **α(OHex)R_2** series), where the emission spectra have detailed structure (in THF). A series of variable polarity solvents was used to elucidate the extent, and type, of solvatochromism. The absorption spectra of **β(O*i*-Pent)$(PhCF_3)_2$** display a weak hypsochromic shift ($\Delta\lambda_{abs}$ = 4 nm), with a larger (albeit still weak) bathochromic shift ($\Delta\lambda_{em}$ = 9 nm) observed in the emission spectra (Fig. 7). This solvatochromism is well-correlated with the solvent polarity parameter, $E_T(30)$,[86] with r^2 values of 0.98 and 0.87 for the absorption and emission spectra respectively. It should be noted that $E_T(30)$ values for binary solvent mixtures such as THF·MeCN, used here as the maximum polarity solvent, are quite complex[87] and the value used here (based on mole fractions) is an approximation. However, it is apparent that this solvatochromism trend is due to the stabilization of the excited state in polar solvent, which in turn yields a larger Stokes shift as solvent polarity increases (Table 3). The A–D–A alignment of **β(O*i*-Pent)$(PhCF_3)_2$** in tandem with the modest Stokes shift (≈10–20 nm) observed imply that the excited state geometry is quite rigid due to the push–pull of the intramolecular charge transfer.[88] Photoluminescence quantum yields for each solvent are given in Table 3 for **β(O*i*-Pent)$(PhCF_3)_2$**, which are in-line with the positive fluorosolvatochromism observed in Miyazaki and co-workers systems.[22]

Table 2 β(O*i*-Pent)R_2 Series spectral data[a]

β(O*i*-Pent)R_2	ε (M^{-1} cm^{-1})	$\lambda_{abs,max}$ (nm)	$E_{g,opt}$[b] (eV)	λ_{em}[c] (nm)	Φ_{PL}[c]
β(O*i*-Pent)Ph_2	4.98×10^4	331	3.22	418	0.16
β(O*i*-Pent)Tol_2	4.31×10^4	330	3.22	420	0.16
β(O*i*-Pent)(PhOMe)$_2$	6.25×10^4	331	3.21	421	0.20
β(O*i*-Pent)$(PhCF_3)_2$	4.40×10^4	342	3.10	432	0.23

[a] UV-visible and emission spectra were measured as solutions in dry, degassed THF under inert atmosphere. [b] $E_{g,opt}$ estimated from the tangent of the absorption onset, $\lambda_{abs,onset}$. [c] λ_{ex} = 365 nm.

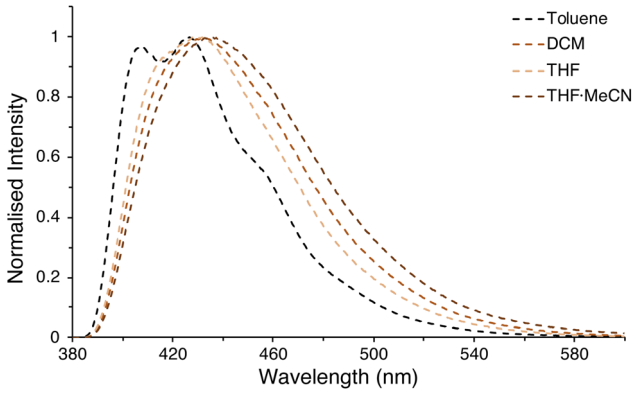

Fig. 7 Fluorosolvatochromism observed for β(O*i*-Pent)(PhCF$_3$)$_2$.

Table 3 Solvatochromism analysis of β(O*i*-Pent)(PhCF$_3$)$_2$[a]

Solvent	$E_T(30)$ (kcal mol^{-1})	ε (M^{-1} cm^{-1})	$\lambda_{abs,max}$ (nm)	λ_{em}[b] (nm)	Φ_{PL}[b]
Tol	33.9	4.37×10^4	343	426	0.18
DCM	40.7	4.68×10^4	340	432	0.17
THF	37.4	4.35×10^4	341	432	0.23
THF·MeCN	42.4[c]	4.93×10^4	339	435	0.15

[a] UV-visible and emission spectra were measured as solutions in dry, degassed solvents under inert atmosphere. [b] $\lambda_{ex} = 365$ nm. [c] Weighed by mole fraction of 1 : 1 solvent mixture.

3 Conclusions

In summary, two isomeric sets of bent naphthodithiophenes have been synthesized and characterized as photoactive small molecules. In both the **α(OR′)R$_2$** and **β(O*i*-Pent)R$_2$** series structural authentication in the solid-state show that the end-caps do not impact inter-ring bond lengths, yet solution-state measurements made *via* NMR spectroscopy show minor perturbations of interior resonances far removed from the **R**-groups. In the **α(OHex)R$_2$** series spectrophotometry measurements detail fine vibronic structure across all derivatives with modest photoluminescence quantum yields ($\Phi_{PL} \approx 0.24$–0.40). Alternatively, the **β(O*i*-Pent)R$_2$** series are far less luminescent due to the limited conjugation path brought on by the orientation of the thiophene moieties. Attachment of electron donating groups has negligible impact on the properties of the fluorophores, but electron deficient groups have a distinct response to their A–D–A motif. **β(O*i*-Pent)(PhCF$_3$)$_2$** displays positive fluorosolvatochromism and becomes broadened as solvent polarity increases, indicative of increased intramolecular charge transfer character. The photophysical characterization of these isomeric bent NDTs highlights how these simple fluorophores have unique applications as photoactive small molecules. Efforts to maximize the effective conjugation path of these isomeric bent NDTs in small molecule systems and determine their applications in organic electronics are underway.

Data availability

The data supporting this article have been included as part of the ESI.†

Author contributions

Z. J. K. conceptualized the project and acquired funding to carry out the experimental portion of the research. E. B. A. A, C. D. G., M. C., D. A., J. P., and Z. J. K. carried out the synthesis, characterization, and spectral analysis of compounds. V. C. and A. R. performed the computations to support the experimental findings and elucidate other parameters of interest. M. Z. carried out the crystallographic analysis. E. B. A. A. and Z. J. K wrote the original draft, with all authors participating in the review and editing process. All authors have given approval to the final version of the manuscript, their respective contributions, and have agreed to publish this work.

Conflicts of interest

There are no conflicts to declare.

Acknowledgements

Z. J. K., E. B. A. A, C. D. G., M. C., D. A., and J. P. acknowledge support by the National Science Foundation (CHE-2316854) and Oakland University. A. A. R. thanks the Biomedical Research Center at Oakland University for support through the Research Excellence Program. High-performance computing facilities at Oakland University were provided *via* collaboration between the Oakland University Research Office and University Technology Services. M. Z. acknowledges the National Science Foundation Major Research Instrumentation grant (CHE-1625543) for funds used to purchase the single crystal X-ray diffractometer.

Notes and references

1 J. E. Anthony, Functionalized Acenes and Heteroacenes for Organic Electronics, *Chem. Rev.*, 2006, **106**, 5028–5048.
2 W. Jiang, Y. Li and Z. Wang, Heteroarenes as high performance organic semiconductors, *Chem. Soc. Rev.*, 2013, **42**, 6113–6127.
3 X. Guo, M. Baumgarten and K. Müllen, Designing π-conjugated polymers for organic electronics, *Prog. Polym. Sci.*, 2013, **38**, 1832–1908.
4 *Main Group Strategies towards Functional Hybrid Materials*, ed. T. Baumgartner and F. Jäkle, John Wiley & Sons, Inc., 1st edn, 2018.
5 K. Takimiya, I. Osaka and M. Nakano, π-building blocks for organic electronics: Revaluation of "inductive" and "resonance" Effects of π-electron deficient units, *Chem. Mater.*, 2014, **26**, 587–593.
6 S. C. Rasmussen, S. J. Evenson and C. B. McCausland, Fluorescent thiophene-based materials and their outlook for emissive applications, *Chem. Commun.*, 2015, **51**, 4528–4543.

7 S. Shinamura, I. Osaka, E. Miyazaki, A. Nakao, M. Yamagishi, J. Takeya and K. Takimiya, Linear- and angular-shaped naphthodithiophenes: Selective synthesis, properties, and application to organic field-effect transistors, *J. Am. Chem. Soc.*, 2011, **133**, 5024–5035.

8 K. Takimiya and I. Osaka, Naphthodithiophenes: Emerging building blocks for organic electronics, *Chem. Rec.*, 2015, **15**, 175–188.

9 I. Osaka, S. Shinamura, T. Abe and K. Takimiya, Naphthodithiophenes as building units for small molecules to polymers; A case study for in-depth understanding of structure–property relationships in organic semiconductors, *J. Mater. Chem. C*, 2013, **1**, 1297–1304.

10 K. Zhang, J. Zhang, X. Zhang, G. Yu and M. S. Wong, Synthesis and characterization of novel push-pull oligomer based on naphthodithiophene-benzothiodiazole for OFETs application, *Tetrahedron Lett.*, 2018, **59**, 641–644.

11 L. Zhao, Y. Cao, H. Qin, X. He, Z. Zhao, Y. Guo and H. Chen, Synthesis and charge-transport properties of novel π-conjugated polymers incorporating core-extended naphtho [2,1-*b*:3,4-*b*′] dithiophene diimides, *Polym. Chem.*, 2024, **15**, 59–70.

12 H. D. Pham, H. Hu, F. L. Wong, C. S. Lee, W. C. Chen, K. Feron, S. Manzhos, H. Wang, N. Motta, Y. M. Lam and P. Sonar, Acene-based organic semiconductors for organic light-emitting diodes and perovskite solar cells, *J. Mater. Chem. C*, 2018, **6**, 9017–9029.

13 M. Löbert, A. Mishra, C. Uhrich, M. Pfeiffer and P. Bäuerle, Synthesis and characterization of benzo- and naphtho[2,1-*b*:3,4-*b*′] dithiophene-containing oligomers for photovoltaic applications, *J. Mater. Chem. C*, 2014, **2**, 4879–4892.

14 J. Zhu, Z. Ke, Q. Zhang, J. Wang, S. Dai, Y. Wu, Y. Xu, Y. Lin, W. Ma, W. You and X. Zhan, Naphthodithiophene-Based Nonfullerene Acceptor for High-Performance Organic Photovoltaics: Effect of Extended Conjugation, *Adv. Mater.*, 2018, **30**, 1–7.

15 X. Wang, L. Guo, P. F. Xia, F. Zheng, M. S. Wong and Z. Zhu, Dye-sensitized solar cells based on organic dyes with naphtho[2,1-*b*:3,4-*b*′] dithiophene as the conjugated linker, *J. Mater. Chem. A*, 2013, **1**, 13328–13336.

16 H. A. Lin, N. Mitoma, L. Meng, Y. Segawa, A. Wakamiya and K. Itami, Hole-transporting materials based on thiophene-fused arenes from sulfur-mediated thienannulations, *Mater. Chem. Front.*, 2018, **2**, 275–280.

17 C. C. Hsu, K. M. Lee, X. W. Wu, L. Lin, W. L. Yu and C. Y. Liu, Hole-Transporting Materials based on Oligo(hetero)aryls with a Naphthodithiophene Core – Succinct Synthesis by Twofold Direct CH Olefination, *Chem.–Eur. J.*, 2024, **30**, e202302552.

18 X. Shen, X. Lai, H. Lai, T. Zhao, Y. Zhu, M. Pu, H. Wang, P. Tan and F. He, Isomerism Strategy to Optimize Aggregation and Morphology for Superior Polymer Solar Cells, *Macromolecules*, 2022, **55**, 6384–6393.

19 M. Su, M. Lin, S. Mo, J. Chen, X. Shen, Y. Xiao, M. Wang, J. Gao, L. Dang, X.-c. Huang, F. He and Q. Wu, Manipulating the Alkyl Chains of Naphthodithiophene Imide-Based Polymers to Concurrently Boost the Efficiency and Stability of Organic Solar Cells, *ACS Appl. Mater. Interfaces*, 2023, **15**, 37371–37380.

20 L. Meng, T. Fujikawa, M. Kuwayama, Y. Segawa and K. Itami, Thiophene-Fused -Systems from Diarylacetylenes and Elemental Sulfur, *J. Am. Chem. Soc.*, 2016, **138**, 10351–10355.

21 A. Meyer, E. Sigmund, F. Luppertz, G. Schnakenburg, I. Gadaczek, T. Bredow, S. S. Jester and S. Höger, Syntheses and properties of thienyl-substituted dithienophenazines, *Beilstein J. Org. Chem.*, 2010, **6**, 1180–1187.

22 T. Miyazaki, T. Tsutsumi and O. Hayashida, Fluorosolvatochromic Behavior of 2,3-Naphthalimides Expanded by Double Fusion with Benzothiophene and Benzofuran Units, *ChemistrySelect*, 2023, **8**, 6–11.

23 M. Klikar, P. Solanke, J. Tydlitát and F. Bureš, Alphabet-Inspired Design of (Hetero)Aromatic Push–Pull Chromophores, *Chem. Rec.*, 2016, 1886–1905.

24 F. Bureš, Fundamental aspects of property tuning in push–pull molecules, *RSC Adv.*, 2014, **4**, 58826–58851.

25 D. Chaudhuri, E. Sigmund, A. Meyer, L. Röck, P. Klemm, S. Lautenschlager, A. Schmid, S. R. Yost, T. Vanvoorhis, S. Bange, S. Höger and J. M. Lupton, Metal-free OLED triplet emitters by side-stepping Kasha's rule, *Angew. Chem., Int. Ed.*, 2013, **52**, 13449–13452.

26 W. Ratzke, L. Schmitt, H. Matsuoka, C. Bannwarth, M. Retegan, S. Bange, P. Klemm, F. Neese, S. Grimme, O. Schiemann, J. M. Lupton and S. Höger, Effect of Conjugation Pathway in Metal-Free Room-Temperature Dual Singlet-Triplet Emitters for Organic Light-Emitting Diodes, *J. Phys. Chem. Lett.*, 2016, **7**, 4802–4808.

27 J. P. Gallivan and G. B. Schuster, Aggregates of Hexakis(*n*-hexyloxy)triphenylene Self-Assemble in Dodecane Solution: Intercalation of (-)-Menthol 3,5-Dinitrobenzoate Induces Formation of Helical Structures, *J. Org. Chem.*, 1995, **60**, 2423–2429.

28 M. Kohn, Bromination of Catechol, *J. Am. Chem. Soc.*, 1951, **73**, 480.

29 A. A. Sarhan and C. Bolm, Iron(iii) chloride in oxidative C–C coupling reactions, *Chem. Soc. Rev.*, 2009, **38**, 2730–2744.

30 C. Hansch, A. Leo and R. W. Taft, A Survey of Hammett Substituent Constants and Resonance and Field Parameters, *Chem. Rev.*, 1991, **91**, 165–195.

31 B. Wang, J. Zhang, H. L. Tam, B. Wu, W. Zhang, M. S. Chan, F. Pan, G. Yu, F. Zhu and M. S. Wong, Impact of alkyl side chains on the photovoltaic and charge mobility properties of naphthodithiophene-benzothiadiazole copolymers, *Polym. Chem.*, 2014, **5**, 836–843.

32 G. Barbarella, M. Zambianchi, A. Bongini and L. Antolini, The Deformability of the Thiophene Ring: A Key to the Understanding of the Conformational Properties of Oligo- and Polythiophenes, *Adv. Mater.*, 1993, **5**, 834–838.

33 BindFit v0.5, **http://app.supramolecular.org/bindfit/**.

34 D. Brynn Hibbert and P. Thordarson, The death of the Job plot, transparency, open science and online tools, uncertainty estimation methods and other developments in supramolecular chemistry data analysis, *Chem. Commun.*, 2016, **52**, 12792–12805.

35 K. Wolinski, J. F. Hinton and P. Pulay, Efficient implementation of the gauge-independent atomic orbital method for NMR chemical shift calculations, *J. Am. Chem. Soc.*, 1990, **112**, 8251–8260.

36 J. R. Cheeseman, G. W. Trucks, T. A. Keith and M. J. Frisch, A comparison of models for calculating nuclear magnetic resonance shielding tensors, *J. Chem. Phys.*, 1996, **104**, 5497–5509.

37 M. J. Frisch, G. W. Trucks, H. B. Schlegel, G. E. Scuseria, M. A. Robb, J. R. Cheeseman, G. Scalmani, V. Barone, G. A. Petersson, H. Nakatsuji, X. Li, M. Caricato, A. V. Marenich, J. Bloino, B. G. Janesko, R. Gomperts, B. Mennucci, H. P. Hratchian, J. V. Ortiz, A. F. Izmaylov, J. L. Sonnenberg, D. Williams-Young, F. Ding, F. Lipparini, F. Egidi, J. Goings, B. Peng, A. Petrone, T. Henderson, D. Ranasinghe, V. G. Zakrzewski, J. Gao, N. Rega, G. Zheng, W. Liang, M. Hada, M. Ehara, K. Toyota, R. Fukuda, J. Hasegawa, M. Ishida, T. Nakajima, Y. Honda, O. Kitao, H. Nakai, T. Vreven, K. Throssell, J. A. Montgomery Jr, J. E. Peralta, F. Ogliaro, M. J. Bearpark, J. J. Heyd, E. N. Brothers, K. N. Kudin, V. N. Staroverov, T. A. Keith, R. Kobayashi, J. Normand, K. Raghavachari, A. P. Rendell, J. C. Burant, S. S. Iyengar, J. Tomasi, M. Cossi, J. M. Millam, M. Klene, C. Adamo, R. Cammi, J. W. Ochterski, R. L. Martin, K. Morokuma, O. Farkas, J. B. Foresman and D. J. Fox, *Gaussian 16 Revision C.01*, Gaussian Inc. Wallingford CT, 2016.

38 J. Vícha, S. Komorovsky, M. Repisky, R. Marek and M. Straka, Relativistic Spin–Orbit Heavy Atom on the Light Atom NMR Chemical Shifts: General Trends Across the Periodic Table Explained, *J. Chem. Theory Comput.*, 2018, **14**, 3025–3039.

39 J. Vıcha, J. Novotný, S. Komorovsky, M. Straka, M. Kaupp and R. Marek, Relativistic Heavy-Neighbor-Atom Effects on NMR Shifts: Concepts and Trends Across the Periodic Table, *Chem. Rev.*, 2020, **120**, 7065–7103.

40 I. G. Shenderovich, The Scope of the Applicability of Non-relativistic DFT Calculations of NMR Chemical Shifts in Pyridine-Metal Complexes for Applied Applications, *ChemPhysChem*, 2024, **25**, e202300986.

41 I. L. Rusakova and Y. Y. Rusakov, Relativistic Effects from Heavy Main Group p-Elements on the NMR Chemical Shifts of Light Atoms: From Pioneering Studies to Recent Advances, *Magnetochemistry*, 2023, **9**, 24.

42 P. Pyykkö, A. Görling and N. Rösch, A transparent interpretation of the relativistic contribution to the N.M.R. 'heavy atom chemical shift', *Mol. Phys.*, 1987, **61**, 195–205.

43 A. D. Becke, Density-functional thermochemistry. III. The role of exact exchange, *J. Chem. Phys.*, 1993, **98**, 5648–5652.

44 P. J. Stephens, F. J. Devlin, C. F. Chabalowski and M. J. Frisch, Ab Initio Calculation of Vibrational Absorption and Circular Dichroism Spectra Using Density Functional Force Fields, *J. Phys. Chem.*, 1994, **98**, 11623–11627.

45 Z. S. Safi and N. Wazzan, DFT calculations of 1H- and 13C-NMR chemical shifts of 3-methyl-1-phenyl-4-(phenyldiazenyl)-1H-pyrazol-5-amine in solution, *Sci. Rep.*, 2022, **12**, 17798.

46 J. Li, J.-K. Liu and W.-X. Wang, GIAO 13C NMR Calculation with Sorted Training Sets Improves Accuracy and Reliability for Structural Assignation, *J. Org. Chem.*, 2020, **85**, 11350–11358.

47 P. Gao, J. Zhang, Q. Peng, J. Zhang and V.-A. Glezakou, General Protocol for the Accurate Prediction of Molecular 13C/1H NMR Chemical Shifts *via* Machine Learning Augmented DFT, *J. Chem. Inf. Model.*, 2020, **60**, 3746–3754.

48 D. Xin, C. A. Sader, O. Chaudhary, P.-J. Jones, K. Wagner, C. S. Tautermann, Z. Yang, C. A. Busacca, R. A. Saraceno, K. R. Fandrick, N. C. Gonnella, K. Horspool, G. Hansen and C. H. Senanayake, Development of a 13C NMR Chemical Shift Prediction Procedure Using B3LYP/cc-pVDZ and Empirically Derived Systematic Error Correction Terms: A Computational Small Molecule Structure Elucidation Method, *J. Org. Chem.*, 2017, **82**, 5135–5145.

49 A. Bose, G. A. Valdivia-Berroeta and N. C. Gonnella, Predicting Autoxidation of Sulfides in Drug-like Molecules Using Quantum Mechanical/Density Functional Theory Methods, *J. Chem. Inf. Model.*, 2024, **64**, 128–137.

50 D. Xin, C. A. Sader, U. Fischer, K. Wagner, P.-J. Jones, M. Xing, K. R. Fandrick and N. C. Gonnella, Systematic investigation of DFT-GIAO 15N NMR chemical shift prediction using B3LYP/cc-pVDZ: application to studies of regioisomers, tautomers, protonation states and N-oxides, *Org. Biomol. Chem.*, 2017, **15**, 928–936.

51 J. Li, J. Liang, Z. Wang, A. L. Ptaszek, X. Liu, B. Ganoe, M. Head-Gordon and T. Head-Gordon, Highly Accurate Prediction of NMR Chemical Shifts from Low-Level Quantum Mechanics Calculations Using Machine Learning, *J. Chem. Theory Comput.*, 2024, **20**, 2152–2166.

52 M. A. Iron, Evaluation of the Factors Impacting the Accuracy of 13C NMR Chemical Shift Predictions using Density Functional Theory–The Advantage of Long-Range Corrected Functionals, *J. Chem. Theory Comput.*, 2017, **13**, 5798–5819.

53 G. L. Stoychev, A. A. Auer and F. Neese, Efficient and Accurate Prediction of Nuclear Magnetic Resonance Shielding Tensors with Double-Hybrid Density Functional Theory, *J. Chem. Theory Comput.*, 2018, **14**, 4756–4771.

54 S. Li, W. Zhou, H. Gao and Z. Zhou, Density functional theory study of 13C NMR chemical shift of chlorinated compounds, *Magn. Reson. Chem.*, 2012, **50**, 106–113.

55 R. Jain, T. Bally and P. R. Rablen, Calculating Accurate Proton Chemical Shifts of Organic Molecules with Density Functional Methods and Modest Basis Sets, *J. Org. Chem.*, 2009, **74**, 4017–4023.

56 T. Bally and P. R. Rablen, Quantum-chemical simulation of 1H NMR spectra. 2. Comparison of DFT-based procedures for computing proton-proton coupling constants in organic molecules, *J. Org. Chem.*, 2011, **76**, 4818–4830.

57 A. Bagno, F. Rastrelli and G. Saielli, Predicting 13C NMR Spectra by DFT Calculations, *J. Phys. Chem. A*, 2003, **107**, 9964–9973.

58 D. Flaig, M. Maurer, M. Hanni, K. Braunger, L. Kick, M. Thubauville and C. Ochsenfeld, Benchmarking Hydrogen and Carbon NMR Chemical Shifts at HF, DFT, and MP2 Levels, *J. Chem. Theory Comput.*, 2014, **10**, 572–578.

59 A. M. Teale, O. B. Lutnæs, T. Helgaker, D. J. Tozer and J. Gauss, Benchmarking density-functional theory calculations of NMR shielding constants and spin–rotation constants using accurate coupled-cluster calculations, *J. Chem. Phys.*, 2013, **138**, 024111.

60 R. J. Iuliucci, J. D. Hartman and G. J. O. Beran, Do Models beyond Hybrid Density Functionals Increase the Agreement with Experiment for Predicted NMR Chemical Shifts or Electric Field Gradient Tensors in Organic Solids?, *J. Phys. Chem. A*, 2023, **127**, 2846–2858.

61 W.-J. Ai, J. Li, D. Cao, S. Liu, Y.-Y. Yuan, Y. Li, G.-S. Tan, K.-P. Xu, X. Yu, F. Kang, Z.-X. Zou and W.-X. Wang, A Very Deep Graph Convolutional Network for 13C NMR Chemical Shift Calculations with Density Functional Theory Level Performance for Structure Assignment, *J. Nat. Prod.*, 2024, **87**, 743–752.

62 I. M. Novitskiy and A. G. Kutateladze, DU8ML: Machine Learning-Augmented Density Functional Theory Nuclear Magnetic Resonance Computations for High-Throughput *In Silico* Solution Structure Validation and Revision of Complex Alkaloids, *J. Org. Chem.*, 2022, **87**, 4818–4828.

63 W. Yan and X. Xu, Accurate Prediction of Nuclear Magnetic Resonance Parameters *via* the XYG3 Type of Doubly Hybrid Density Functionals, *J. Chem. Theory Comput.*, 2022, **18**, 2931–2946.

64 J. B. K. Büning and S. Grimme, Computation of CCSD(T)-Quality NMR Chemical Shifts *via* Δ-Machine Learning from DFT, *J. Chem. Theory Comput.*, 2023, **19**, 3601–3615.

65 F. Jensen, How Large is the Elephant in the Density Functional Theory Room?, *J. Phys. Chem. A*, 2017, **121**, 6104–6107.

66 B. Nagy and F. Jensen, *Reviews in Computational Chemistry*, Reviews in Computational Chemistry, 2018, pp. 93–149.

67 F. Jensen, Computational Chemistry: The Exciting Opportunities and the Boring Details, *Isr. J. Chem.*, 2022, **62**, year.

68 F. Jensen, Unifying General and Segmented Contracted Basis Sets. Segmented Polarization Consistent Basis Sets, *J. Chem. Theory Comput.*, 2014, **10**, 1074–1085.

69 F. Jensen, Segmented Contracted Basis Sets Optimized for Nuclear Magnetic Shielding, *J. Chem. Theory Comput.*, 2015, **11**, 132–138.

70 A. E. A. Fouda and N. A. Besley, Assessment of basis sets for density functional theory-based calculations of core-electron spectroscopies, *Theor. Chem. Acc.*, 2017, **137**, 6.

71 R. T. Ireland and L. K. McKemmish, On the specialization of Gaussian basis sets for core-dependent properties, *J. Chem. Phys.*, 2023, **159**, 064102.

72 G. I. Warren, J. E. Barker, L. N. Zakharov and M. M. Haley, Enhancing the Antiaromaticity of s-Indacene through Naphthothiophene Fusion, *Org. Lett.*, 2021, **23**, 5012–5017.

73 Z. Chen, C. S. Wannere, C. Corminboeuf, R. Puchta, V. Ragué and P. Schleyer, Nucleus-independent chemical shifts (NICS) as an aromaticity criterion, *Chem. Rev.*, 2005, **105**, 3842–3888.

74 R. Gershoni-Poranne and A. Stanger, Magnetic criteria of aromaticity, *Chem. Soc. Rev.*, 2015, **44**, 6597–6615.

75 A. Stanger, NICS – Past and Present, *Eur. J. Org Chem.*, 2020, **2020**, 3120–3127.

76 A. Rahalkar and A. Stanger, *AROMA Package*, 2014, **http://chemistry.technion.ac.il/members/amnon-stanger/**.

77 R. Gershoni-Poranne and A. Stanger, The NICS-XY-scan: Identification of local and global ring currents in multi-ring systems, *Chem.–Eur. J.*, 2014, **20**, 5673–5688.

78 J. D. Tovar and T. M. Swager, Poly(naphthodithiophene)s: Robust, Conductive Electrochromics *via* Tandem Cyclization–Polymerizations, *Adv. Mater.*, 2001, **13**, 1775–1780.

79 D. Xia, A. Keerthi, C. An and M. Baumgarten, Synthesis of a quinoidal dithieno[2,3-d;2,3-d benzo[2,1-*b*;3,4-*b*′]-dithiophene] based open-shell singlet biradicaloid, *Org. Chem. Front.*, 2017, **4**, 18–21.

80 X. A. Cook, A. de Gombert, J. McKnight, L. R. Pantaine and M. C. Willis, The 2-Pyridyl Problem: Challenging Nucleophiles in Cross-Coupling Arylations, *Angew. Chem., Int. Ed.*, 2021, **60**, 11068–11091.

81 J. D. Tovar, A. Rose and T. M. Swager, Functionalizable polycyclic aromatics through oxidative cyclization of pendant thiophenes, *J. Am. Chem. Soc.*, 2002, **124**, 7762–7769.

82 D. Waghray, C. De Vet, K. Karypidou and W. Dehaen, Oxidative transformation to naphthodithiophene and thia [7] helicenes by intramolecular scholl reaction of substituted 1,2-bis(2-thienyl)benzene precursors, *J. Org. Chem.*, 2013, **78**, 11147–11154.

83 W. Wang, X. Li, Z. Qi, B. Ji, Z. Wang, S. Wang and J. Xiao, Synthesis, Crystal Analysis, and Physical Properties of Double [6] helicene-Containing Heteroarenes with Circularly Polarized Luminescence, *Org. Lett.*, 2023, **25**, 1343–1347.

84 E. Clar, *The Aromatic Sextet*, J. Wiley, 1972.

85 M. Solà, Forty years of Clar's aromatic π-sextet rule, *Front. Chem.*, 2013, **1**, 4–11.

86 C. Reichardt, Solvatochromic dyes as solvent polarity indicators, *Chem. Rev.*, 1994, **94**, 2319–2358.

87 S. Nigam and S. Rutan, Principles and Applications of Solvatochromism, *Appl. Spectrosc.*, 2001, **55**, 362A–370A.

88 P. Vázquez-Domínguez, J. F. Rizo, J. F. Arteaga, D. Jacquemin, L. Favereau, A. Ros and U. Pischel, Azaborahelicene fluorophores derived from four-coordinate N,C-boron chelates: synthesis, photophysical and chiroptical properties, Organic, *Chem. Front.*, 2023, **11**, 843–853.